Asphaltene Fractionation Based on Adsorption onto Calcium Carbonate: Part 1. Characterization of Sub-fractions and QCM-D Measurements

Sreedhar Subramanian*, Sébastien Simon, Bicheng Gao and Johan Sjöblom

Ugelstad Laboratory, Department of Chemical Engineering, Norwegian University of Science and Technology (NTNU), N-7491 Trondheim, Norway.

ABSTRACT

A new fractionation procedure was developed based on adsorption of asphaltenes onto calcium carbonate. The fractions obtained were characterized by elemental analysis, Fourier Transform Infrared Spectroscopy (FTIR) and Quartz Crystal Microbalance with Dissipation (QCM-D). FTIR analysis indicated that the sub-fractions obtained differed in the amount of carbonyl, carboxylic acid or derivative groups present in them. The adsorption of these fractions on stainless steel was studied by QCM-D. While the unfractionated asphaltenes exhibited a maximum saturation adsorption (Γ_{max}) of 3.4 mg/m^2, the sub-fractions did not however show a Γ_{max} within the concentration range tested (0.01 - 1.5 g/L). The asphaltene fraction with highest concentration of carbonyl, carboxylic acid or derivative groups formed visco-elastic layers on stainless steel and also exhibited maximum adsorption (around 8 mg/m^2). Finally, results obtained from QCM-D measurement suggest that the interaction of the asphaltene sub-fractions tend to prevent an adsorption of unfractionated asphaltenes onto stainless steel.

KEYWORDS

Asphaltene fractionation, Elemental Analysis, FTIR, QCM-D

1. INTRODUCTION

Asphaltenes are operationally defined as the fraction of crude oil which is soluble in toluene but insoluble in n-heptane.[1, 2] Among the various crude oil constituents, asphaltenes have the highest molecular weight and are also the most polar.[3] It is now recognized that asphaltenes have a broad molecular weight distribution with an average molecular weight of around 750 g/mol with a factor of 2 in width of the molecular weight distribution.[4, 5] The properties of asphaltenes obtained from crude is dependent upon the type of extraction method used.[6] Fractionation is one of the ways to improve the characterization and understanding the properties of asphaltenes. Several methods exist, for instance some researchers[7-14] initially precipitated asphaltenes by diluting with an n-alkane and then used a binary mixture of solvents (polar solvent + anti-solvent) to fractionate the precipitated asphaltenes. Other fractionation procedures less commonly used include fractionation by varying the crude oil/n-alkane ratios[15-18], ultracentrifugation[19, 20], ultrafiltration[14], supercritical extraction[21] and gel permeation chromatography[22, 23]. Yarranton and Masliyah[7] fractionated the asphaltenes from Athabasca bitumens by varying the toluene/n-hexane ratio. They obtained fractions of different molar mass and found that the sub-fraction with higher molar mass had lower solubility. Nalwaya et al.[8] and Kaminski et al.[9] used methylene chloride/n-pentane mixture to fractionate asphaltenes from Mobil crude oil (US) and Chaguaramal crude oil (Venezuela). They observed that the asphaltene sub-fraction with higher polarity showed lower rate of dissolution. The sub-fractions had different texture and crystalline/amorphous nature, but FTIR analysis and molecular weight information could not provide information on their structural differences. Similarly, Groenzin et al.[10] used a mixture of toluene/n-pentane to fractionate asphaltenes and observed that the sub-fractions contained the same molecular species (ie., alkyl chain and aromatic rings) but have different

distribution. Buenrostro-Gonzalez et al.[11] fractionated asphaltenes using toluene/n-heptane and toluene/acetone mixtures and found that the sub-fractions obtained using acetone as precipitant exhibited larger structural differences than compared to sub-fractions obtained with n-heptane. Similarly, Kharrat[12, 13] used THF/n-hexane mixtures to fractionate asphaltenes from Athabasca oil and Morgan Oil and observed that the sub-fraction which precipitates first had more condensed aromatic rings but with less alkyl substitution. Fossen et al.[15, 16] diluted a North Sea crude with different ratios of n-pentane to obtain asphaltene sub-fractions and found that the interfacial activity was higher for sub-fraction which was less aromatic and contained more alcoholic and carboxylic acid groups in the alkyl chain.

Size exclusion chromatography (SEC) or gel permeation chromatography (GPC) is another technique used to fractionate asphaltenes based on their molecular size. The larger molecules percolate through the porous gel bed and hence elute first, while the smaller molecules spend more time inside the gel and hence elute later. The choice of eluent plays an important role in SEC due to interaction of asphaltenes with the stationary phase (or the column). Earlier works[24, 25] were based on tetrahydrofuran (THF) as mobile phase, but partial loss of asphaltene samples as well as material precipitation from solution in THF based SECs have been reported.[26] Another solvent employed as eluent is N-methyl-2-pyrrolidinone (NMP).[27-30] However, while NMP is a good solvent for coal derivatives, the solvency of NMP has been found to be limited for petroleum asphaltenes. NMP insoluble asphaltene fractions have been found to be have larger size than soluble fractions.[31] Similarly, Ascenius et al.[30] observed that the NMP insoluble petroleum asphaltenes do not exhibit fluorescence. The problem of insolubility has however been overcome with use of NMP-chloroform mixture as an eluent. However, use of SEC for fractionating asphaltenes is a challenge due to the need for elaboration of calibration standards, interpretation of the

molecular mass and uncertainty in upper limit of molecular weight determination by SEC.[31]

The polarity of asphaltenes molecules causes them to adsorb onto surfaces.[32] The adsorption of asphaltenes onto surfaces (mineral and metallic) is an undesired phenomena in the petroleum industry as it can lead to formation damage[32], wettability alteration[33], plugging of wells and flow-lines[34, 35]. Several techniques have been used to study the adsorption of asphaltenes onto solid surfaces including quartz crystal microbalance (QCM)[36-38] and UV-vis spectroscopy[39, 40]. The ability of asphaltenes to adsorb as monolayer[41] as well as multiple layers[41-45] has been reported in literature. The nature of adsorption isotherm is dependent on the concentration of the asphaltene solution[45] as well as the choice of solvent used to redissolve asphaltenes[41]. Saturation asphaltene adsorption amounts in range of 0.26 - 3.78 mg/m^2 have been observed on mineral surfaces and this is strongly dependent on the studied surface.[40] Asphaltenes from Athabasca and Cold Lake have shown almost twice as high adsorption onto stainless steel than on iron.[39] Asphaltene adsorption of upto 5 mg/m^2 has been observed on iron oxide surface.[46] However, multilayer adsorption of asphaltenes onto mineral surfaces (Bedford limestone, Berea sandstone and dolomite) with adsorbed values in the range 100 - 200 mg/m^2 at very high asphaltene concentrations in toluene has also been reported.[47] The multilayer step wise asphaltene adsorption has been attributed to the asphaltene association and formation of aggregates.[43]

To the best of our knowledge, only limited studies[48, 49] on the fractionation of asphaltenes based on functionality or polarity has been undertaken since the retention of the asphaltenes onto the solid adsorbent is considered to be a drawback.[50] In the present study, a new

fractionation procedure has been developed based on adsorption of asphaltenes onto $CaCO_3$. The aim of the new procedure is to separate asphaltenes into sub-fractions of reduced polydispersity based on variation in functional groups and to study the influence of polydispersity in functional groups on adsorption characteristics. An attempt has been made to recover most of the asphaltenes retained onto the adsorbent and to obtain a material balance for the entire fractionation procedure. The asphaltene sub-fractions are characterized using elemental analysis and Fourier Transform Infrared Spectroscopy (FTIR) followed by determination of adsorption tendencies of these asphaltene sub-fractions onto stainless steel surface using Quartz Crystal Microbalance with Dissipation (QCM-D) monitoring.

2. EXPERIMENTAL SECTION

2.1 Chemicals

A chemical-free crude oil from the Norwegian Continental shelf was used for extraction of asphaltenes. The characteristics of the crude oil are given in table 1. Asphaltene extraction from crude was done using n-hexane (VWR, >97%). For asphaltene fractionation, precipitated $CaCO_3$ (Speciality Minerals Inc., USA), anhydrous toluene (Sigma Aldrich, 99.8%), anhydrous tetrahydrafuran (VWR, >99.7%), chloroform (Merck, >97%), acetic acid (Sigma Aldrich, >99%) and 4N HCl were used. The 4N HCl solution was prepared by diluting hydrochloric acid fuming (Merck, 37%) with purified water. For QCM measurements, xylene (VWR, >98.5%) were used. The quartz crystals were supplied by biolin scientific. Hellmanex III (Hellma Analytics) and ethanol (VWR, 96%) were solvents used for cleaning crystals.

2.2 Asphaltene Extraction

The crude oil was initially conditioned for 2 hours at 60°C. The crude was then sampled and diluted with excess of n-hexane in the ratio 1:40 (w/v). The mixture was stirred for 24 hours

at 22°C. The precipitated asphaltenes were obtained by filtering the mixture under vacuum using a Millipore 0.45μm filter. The asphaltenes were washed with n-hexane until the filtrate was colorless. The asphaltenes were dried overnight in a dessicator filled with nitrogen gas.The asphaltenes obtained is called as unfractionated or *whole* asphaltenes.

Density at 15°C (g/cm^3)	TAN (mg/g)	TBN (mg/g)	Water content (wt%)	SARA analysis (wt%)			
				Saturates	Aromatics	Resins	Asphaltenes
0.939	2.15	2.81	0.11	37	44	16	2.5

Table 1: Characteristics of crude oil used in this work.[51]

2.3 Calcium Carbonate

The properties of the $CaCO_3$ used in the study are given in table 2. The particle size was provided by the supplier. The BET surface area of the $CaCO_3$ particles was determined by N_2 adsorption method[40] while the structure of particle was determined by x-ray diffraction (XRD)[52].

Particle size (μm)	0.07
Form	Calcite
BET surface area (m^2/g)	18.1 ± 0.3

Table 2: Properties of $CaCO_3$

2.4 Determination of fractionation parameters

A series of 10 ml solutions of *whole* asphaltenes in toluene were prepared in the concentration (C_o) range 0.1 g/L - 6 g/L with 550 mg of $CaCO_3$ added to each solution. The solutions were stirred at room temperature (22°C) for 24 hours and then centrifuged at 4000 rpm for 20 min. The concentration of asphaltene in the supernatant was determined using UV

spectroscopy (described in section 2.6). The amount of asphaltene adsorbed on $CaCO_3$ was calculated based on the difference in concentration of asphaltenes before and after the adsorption.[40]

2.5 Asphaltene Fractionation

The asphaltenes were fractionated into three sub-fractions based on procedure shown in figure 1.

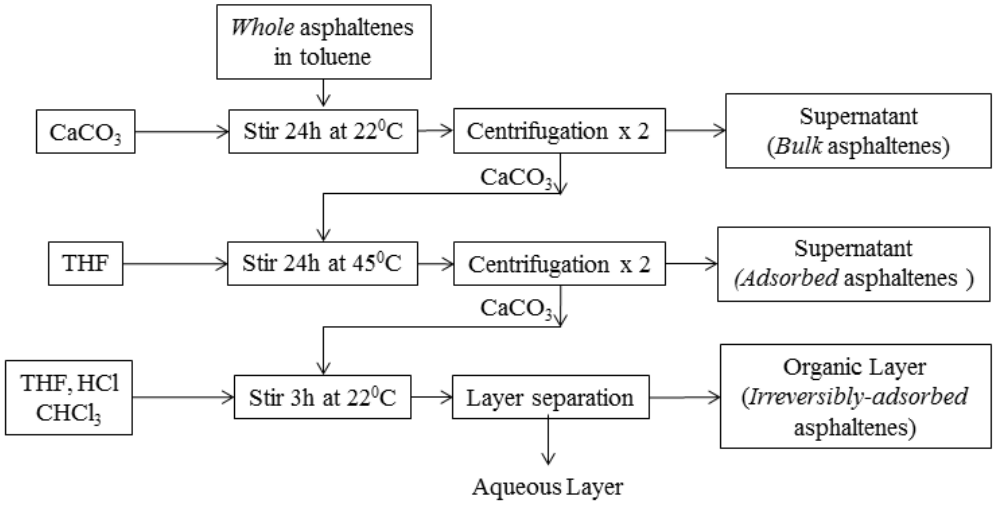

Figure 1: Asphaltene fractionation procedure

(Note: centrifugation x 2 refers to centrifugation being performed twice)

Initially, 4 g/L asphaltene solution was prepared by dissolving 1.5g of *whole* asphaltenes in 375 ml of toluene and sonicating for 30 minutes. $CaCO_3$ (41.4g) was then added to the asphaltene solution and stirred for 24 hours at room temperature (22°C). The solution was then centrifuged at 4000 rpm for 20 min. The supernatant was filtered and concentrated to dryness. The first asphaltene fraction obtained is called *bulk* asphaltenes. Next, 375ml of THF was added to the $CaCO_3$ (remaining after centrifugation containing asphaltenes adsorbed) and the solution was stirred for 24 hours at 45°C followed by centrifugation at 4000 rpm for 20

min. The supernatant was recovered, filtered and concentrated to dryness. The asphaltene fraction obtained was redissolved in toluene and then concentrated to dryness. The second asphaltene fraction obtained is called *adsorbed* asphaltenes. 750ml of mixture consisting of 50/50 (v/v) THF/$CHCl_3$ was added to the remaining $CaCO_3$ (after centrifugation) followed by slow addition of 4N HCl solution (750 ml). The solution was allowed to stir for 3 hours at room temperature. The organic and aqueous layers were separated. The organic layer was then washed with water and concentrated to dryness. The asphaltene fraction obtained was redissolved in toluene and then concentrated to dryness. The asphaltene fraction obtained is called as *irreversibly-adsorbed* asphaltenes. All the asphaltene sub-fractions were dried in a block heater (Grant UBR) maintained at 70°C under a stream of nitrogen.

2.6 UV spectroscopy

The concentration of asphaltenes in toluene was determined using UV spectroscopy by building up a calibration curve with the *whole* asphaltenes at wavelength 336nm. Thereafter the solutions of asphaltene sub-fraction (*bulk*, *adsorbed*, *irreversibly-adsorbed*) in toluene were diluted before measurement so that they are within the calibration range.

2.7 Elemental Analysis

The elemental composition (C, H, N, O, S) and metal content (Fe, Ni, V, Ca, Na, K) of the crude oil and the asphaltene fractions was determined by Laboratory SGS Multilab (Evry, France) by thermal conductivity measurements for C, H and N, infrared measurements for O and S, and ICP-AE measurements after mineralization in bomb Milestone by microwave for metal content.

2.8 Fourier Transform Infrared Spectroscopy (FTIR)

The Tensor 27 spectrometer (Bruker Optics) equipped with a Bruker Golden Gate diamond Attenuated Total Reflection (ATR) cell was used to record the FTIR spectra of the samples in the spectral range 4000 to 600 cm^{-1}, with 4 cm^{-1} resolution. The asphaltene samples were dissolved in CH_2Cl_2 and small amounts of sample was placed on the cell. The measurements were done after the solvent had completely evaporated.

2.9 Quartz Crystal Microbalance with Dissipation (QCM-D) Measurements

The adsorption of asphaltenes onto quartz crystal coated with stainless steel was measured using QCM-D. The apparatus used was single sensor microbalance system Q-sense E1 from Biolin Scientific (Sweden). The XPS composition of the stainless steel coating on quartz crystal is given in table 3.

Element	Atomic (%)
Fe	36.5
Cr	8.0
Mn	1.0
O	53.7

Table 3: Composition of stainless steel coating by XPS (provided by the manufacturer).

The crystals were cleaned prior to use as per the following protocol: the crystal was immersed in 1% hellmanex solution in water for at least 1 hour followed by washing with purified water, sonication in ethanol for 10 min, drying with N_2 and finally treatment in UV chamber for 15 min.

QCM adsorption experiments were performed with the following procedure: xylene is initially passed through the chamber containing crystal at 20°C to obtain a baseline. The

baseline was considered to be stable if the frequency change was less than ±1 Hz for 10 min. Solutions of asphaltene in xylene were then injected into the chamber in a stepwise manner using a pump (flow rate = 750 µL/min). Sample injection time was 10 min followed by a waiting time of 5 min before the next sample injection was performed. Desorption study was done by injecting xylene after passing the most concentrated asphaltene solution. The QCM experiments were repeated at least twice for each measurement.

The QCM-D operates based on the property of piezoelectricity. The piezoelectric quartz crystal coated with stainless steel is located between the two metal electrodes. By applying an AC voltage across the electrodes, the crystal is excited to oscillate. The frequency of oscillation is dependent on the mass adsorbed onto the surface of the crystal. The relationship between the change in frequency (Δf) due to the mass adsorbed (Δm) was established by Sauerbrey[53] as (equation 1)

$$\Delta m = -\frac{\rho_q t_q}{f_o n}\Delta f = -\frac{\rho_q v_q}{2 f_o^2 n}\Delta f = -\frac{C}{n}\Delta f \quad (1)$$

Where ρ_q (=2648 kg/m^3) and t_q (=0.33 mm) are the mass density and thickness of the crystal, v_q (=3340 m/s) is shear wave velocity in quartz, f_o (= 5 MHz) is the fundamental frequency of crystal and n is the overtone number. The constant C equals 0.177 mg/m^{2}Hz. In the present study, the overtones 3, 5 and 7 are considered. The Sauerbrey equation is valid only when the mass adsorbed is evenly distributed on the surface, Δm is smaller than the mass of the crystal and the adsorbed mass is rigidly attached to the surface.[53]

The change in dissipation due adsorption is given by the relationship[54]

$$D = \frac{E_{disspiated}}{2\pi E_{stored}} \quad (2)$$

Where D is the dissipation factor, $E_{disspiated}$ is the energy dissipated during one period of oscillation and E_{stored} is the energy stored in the oscillating system. In the case of formation of viscoelastic films on the surface, the Sauerbrey's relationship (equation 1) is no longer valid.

3. RESULTS AND DISCUSSION

3.1 Fractional yields

The objective of this study is to develop a fractionation procedure based on adsorption of asphaltenes onto calcium carbonate. At first, the amount of asphaltenes adsorbed onto $CaCO_3$ at different asphaltene solution concentration was determined. Figure 2 shows the variation of adsorbed asphaltene amount as a function of supernatant concentration.

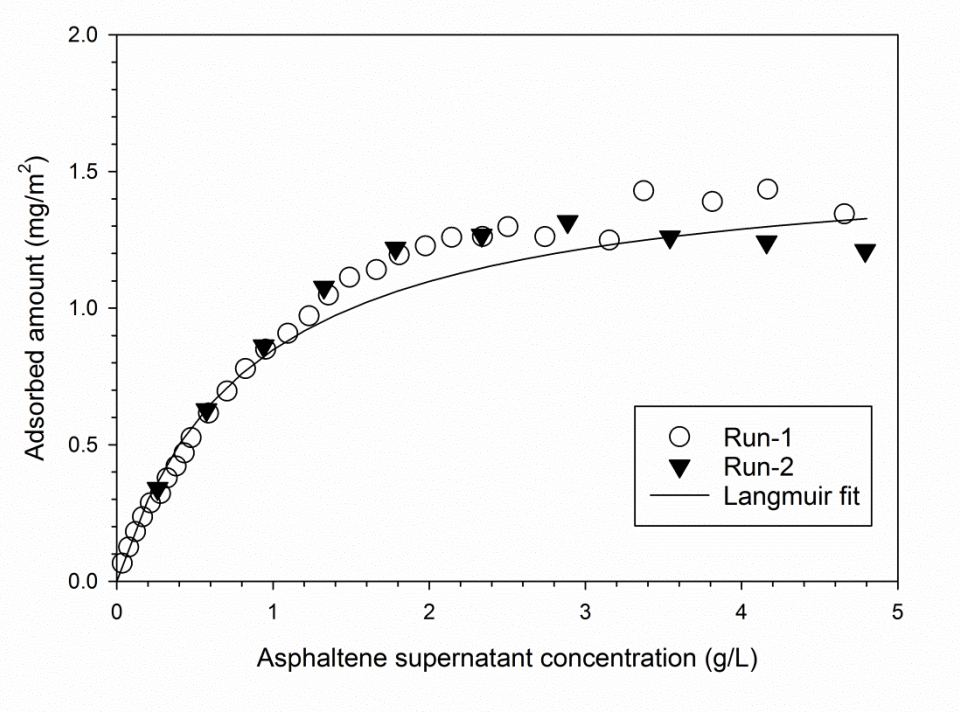

Figure 2: Adsorption of *whole* asphaltenes onto $CaCO_3$ particles

A non-linear increase of the adsorbed amount at low asphaltene concentration is observed. The slope of the curve decreases to reach a plateau at asphaltene concentrations of

approximately 2-3 g/L. No further increase in asphaltene adsorption onto $CaCO_3$ is observed beyond 2-3 g/L asphaltene concentration thereby indicating that the surface is saturated with asphaltenes. Here, the plateau adsorbed amount is consistent with other studies.[40] The adsorption plot in figure 2 allowed us to then determine the conditions of separation reported in the experimental section.

Assuming that there is a monolayer asphaltene adsorption onto $CaCO_3$ and there is no solute-solute or solute-solvent interactions, the shape of adsorption curve was fitted (based on linearization) to the Langmuir equation:

$$\Gamma = \frac{\Gamma_{max} K C}{1 + KC} \tag{3}$$

Where, Γ_{max} is the maximum adsorbed amount and K is the equilibrium constant. The Langmuir fit gave us Γ_{max} = 1.56 mg/m^2 and K = 1.19 L/g. The values obtained were found to be in good agreement with other studies.[40] However, the intrinsic meaning of the Langmuir isotherm parameters needs to be questioned since some asphaltenes were found to be irreversibly adsorbed on calcium carbonate.

The yield of different asphaltene sub-fractions is quantified both by UV-spectroscopy and gravimetry as shown in table 4. The minor difference in the values obtained by the two methods can be attributed to the calibration curve used for UV spectroscopy. The calibration was done with *whole* asphaltenes and it is likely that the asphaltene sub-fractions have a slightly different response factor in UV. The Beer-Lambert's coefficient is high at 336nm and the asphaltene fractionation yields were almost the same when compared at other wavelengths. Hence only the values obtained based on 336 nm is reported in table 4.

Asphaltene sub-fractions	Fractionation yield (wt%)			
	HCl (for acid treatment)		Acetic acid (for acid treatment)	
	UV	Gravimetry	UV	Gravimetry
Bulk	51.2 ± 0.5	49.1 ± 0.3	52.3	51.4
Adsorbed	29.9 ± 1.4	29.4 ± 0.7	27.7	27.4
Irreversibly-adsorbed	17.1 ± 0.6	20.6 ± 1.2	17.3	19.6
Total	98.2 ± 1.2	99.1 ± 1.4	97.4	98.4

Table 4: Asphaltene fractionation yields based on 4 experiments with HCl and 1 experiment with acetic acid.

The first fractionation step consisted of adsorbing 50 wt% of the initial material on $CaCO_3$. It was observed that a significant amount of asphaltenes (around 20 wt%) remained on the $CaCO_3$ even after desorption of asphaltenes from $CaCO_3$ using THF at 45°C. This asphaltene sub-fraction had therefore strong affinity to $CaCO_3$ and treatments involving different temperatures and solvents (chloroform) could not make it desorb from $CaCO_3$. Hence an acid treatment (HCl addition) approach was utilized to remove the $CaCO_3$ which is strongly adsorbed onto the asphaltenes by dissolution (equation 4).

$$CaCO_3 + 2HCl \rightarrow CaCl_2 + H_2O + CO_2 \uparrow \quad (4)$$

The entire separation procedure is quantitative with a recovery of 98-99% (by weight) of the initial asphaltene material. The separation procedure is robust and has good reproducibility with the sub-fraction yields variation in the range ± 1 wt%. Fractionation experiments were also performed using acetic acid instead of HCl in the acid treatment step and the yields were similar.

3.2. Characterization by Elemental Analysis

The elemental analysis of the crude and different asphaltene fractions are listed in table 5. The *whole* asphaltene precipitated from crude oil has a much higher concentration of heteroatoms (N, S, O) in them than compared to the crude oil. The H/C ratio for all the asphaltene fractions varied between a narrow range (1.13 – 1.20) thereby indicating that the fractions have almost similar aromaticity or unsaturation. The *irreversibly-adsorbed* asphaltene sub-fraction shows a slightly higher H/C ratio (around 1.19) indicating that the fraction has a slightly higher aliphatic character compared to remaining fractions. The nitrogen and sulfur contents in all the asphaltene fractions are similar. However, the fractions show a significant variation in oxygen content with *irreversibly-adsorbed* sub-fraction containing the maximum amount of oxygen. It should be noted that the fractionation procedure has led to an increase in the oxygen content in the sub-fractions (*bulk, adsorbed, irreversibly-adsorbed*) than compared to *whole* asphaltenes and this may be due to contamination of asphaltene sub-fractions by $CaCO_3$ or due to oxidation of asphaltenes during the experiment.

The mass balance of elements was calculated from the following equation:

$$\%\ loss\ (or) gain = \left(\frac{f_{bulk}X_{bulk} + f_{adsorbed}X_{adsorbed} + f_{irreversibly}X_{irreversibly} - X_{whole}}{X_{whole}}\right)100 \quad (5)$$

Where,

f_{bulk}, $f_{adsorbed}$ and $f_{irreversibly}$ refers to fractional yield of *bulk*, *adsorbed* and *irreversibly-adsorbed*^{HCl} asphaltenes respectively (based on average value reported in table 4).

X_{whole}, X_{bulk}, $X_{adsorbed}$ and $X_{irreversibly}$ refers to the weight percentage (wt%) of corresponding element in *whole*, *bulk, adsorbed* and *irreversibly-adsorbed*^{HCl} asphaltene fractions respectively.

Element	Crude oil	Asphaltene fractions					
		Whole	*Bulk*	*Adsorbed*	*Irreversibly-adsorbed*^{HCl}	*Irreversibly-adsorbed*^{AA}	% loss or % gain
C (wt%)	86.90	85.60	85.70	84.30	83.40	84.20	-1.7
H (wt%)	11.67	8.17	8.12	8.00	8.30	8.32	-1.5
N (wt%)	0.28	1.32	1.20	1.40	1.35	1.36	-3.0
O (wt%)	0.46	1.85	2.33	3.27	4.22	3.79	+58.4
S (wt%)	0.87	1.96	1.91	2.28	2.14	2.13	+4.5
Total (wt%)	100.18	98.90	99.26	99.25	99.41	99.80	-
H/C ratio (-)	1.610	1.145	1,137	1.139	1.194	1.186	-

Table 5: Elemental analysis of crude oil, *whole* asphaltenes and sub-fractions (*bulk, adsorbed*, *irreversibly-adsorbed*). The superscript *HCl* (hydrochloric acid) and *AA* (acetic acid) refer to acid used to obtain the *irreversibly-adsorbed* sub-fraction. The mass balance of elements in asphaltene (calculated based on equation 5) is indicated by % loss (negative) or % gain (positive).

In order to study the possibility of oxidation of asphaltenes during the fractionation procedure, a control experiment was performed. The control experiment consisted of subjecting *whole* asphaltenes (in absence of $CaCO_3$) to the same sequence of unit operations (stirring, centrifugation, concentration and drying) followed during fractionation procedure to obtain the *irreversibly-adsorbed* asphaltenes. The elemental analysis and metal content of *whole* asphaltenes after control experiment (known as *control* asphaltenes) has been presented in tables S1 and S2 in the supplementary material. An increase in oxygen content (around 21 wt%) was observed in asphaltenes during the fractionation process. Thus the remaining 37 wt% increase in oxygen content (in table 5) can be attributed to $CaCO_3$ contamination.

The metal content in the different asphaltene fractions are given in table 6. The sub-fractions (*bulk* and *adsorbed*) show much higher calcium content than the *whole* asphaltenes. This may again be attributed to the contamination of sub-fractions due to use of $CaCO_3$ for fractionating and is consistent with the higher oxygen content in these two fractions. The *irreversibly-adsorbed* fraction however is not likely to be contaminated by $CaCO_3$ since excess of acid (3 times more than required) is used to obtain this fraction. The sodium content in all the sub-fractions (*bulk, adsorbed* and *irreversibly-adsorbed*) was found to be much lower than the *whole* asphaltenes. The sub-fractions *bulk, adsorbed* and *irreversibly-adsorbed* have much lower Fe content than in *whole* asphaltenes indicating an overall loss of Fe (~75%) during the fractionation. This could most likely be due to removal of some Fe in water phase during the step involving acid treatment and subsequent water washing since Fe has greater solubility in water at lower pH. The variation of vanadium content in *whole, bulk* and *adsorbed* asphaltene fractions was comparatively less, but the *irreversibly-adsorbed* sub-fraction had very low vanadium content. Similarly, the nickel content was found to be lower in *irreversibly-adsorbed* sub-fraction. The fractionation procedure resulted in a small overall loss of vanadium (~15%) and nickel (~13%).

Element	Crude oil	Asphaltene fractions					
		Whole	*Bulk*	*Adsorbed*	*Irreversibly-adsorbed*^{HCl}	*Irreversibly-adsorbed*^{AA}	% loss or % gain
Fe (ppm)	6	96	25	19	<30	<30	-75
V (ppm)	17	256	227	266	128	146	-15
Ni (ppm)	6	77	65	87	40	53	-13
Ca (ppm)	120	1402	6613	3366	655	434	+193
Na (ppm)	<50	641	<218	<192	<250	<250	-66
K (ppm)	<50	<130	<218	<192	<250	<250	-

Table 6: Metal content in crude oil, *whole* asphaltenes and sub-fractions (*bulk*, *adsorbed*, *irreversibly-adsorbed*). The superscript *HCl* (hydrochloric acid) and *AA* (acetic acid) refer to acid used to obtain the *irreversibly-adsorbed* sub-fraction. The mass balance of metals in asphaltene (calculated based on equation 5) is indicated by % loss (negative) or % gain (positive).

3.3. Characterization by FTIR spectrometry

The FTIR spectra obtained from the instrument was baseline corrected by subtracting the absorbance values in the spectra by the absorbance value at 600 cm^{-1}. The baseline corrected spectrum was then normalized by dividing the absorbance values in the spectra by the largest absorbance value. The normalized FTIR spectra of the asphaltene fractions are shown in figures 3. . The spectra presented is divided into two regions: figure 3(a) in spectral range 3200 cm^{-1} to 2600 cm^{-1} and 3(b) in spectral range 2000 cm^{-1} to 600 cm^{-1}.

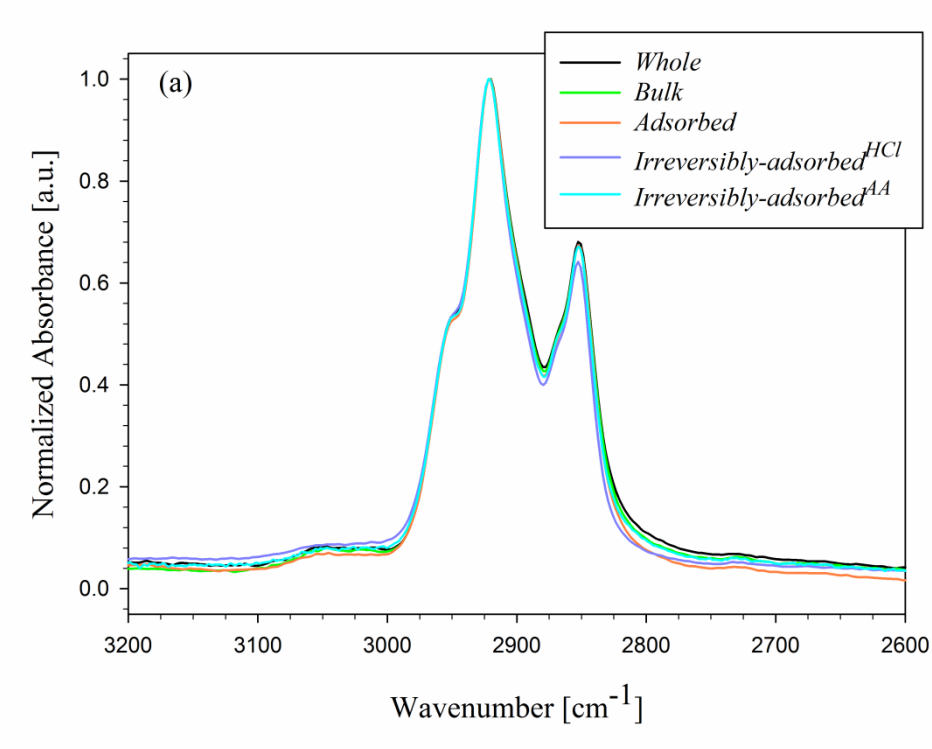

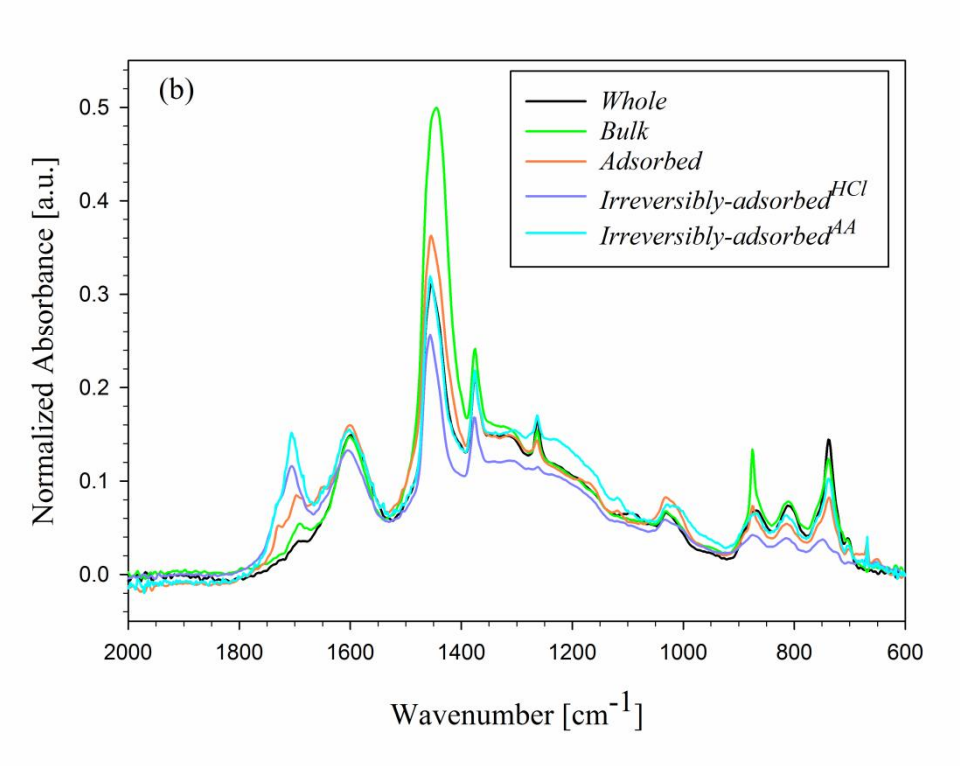

Figure 3: Normalized FTIR spectra of asphaltene fractions (a) spectral range 3200 cm^{-1} to 2600 cm^{-1} (b) spectral range 2000 cm^{-1} to 600 cm^{-1}

The absorbance bands observed between 2950 cm^{-1} and 2830 cm^{-1} correspond to the stretching vibration of respective aliphatic -CH_3 and -CH_2 groups. Figure 3(a) shows that all the asphaltene fractions have similar absorption band characteristics in this spectral range 2950 cm^{-1} and 2830 cm^{-1} thereby indicating presence of similar alkyl groups in fractions. None of the asphaltene fractions exhibited any noticeable stretching in the spectral range 3600 cm^{-1} to 3100 cm^{-1} (not shown in figure) thereby indicating low concentration of molecules with –NH and –OH groups. The band around 1700 cm^{-1} is attributed to the stretching of carbonyl, carboxylic acid or derivative groups. The asphaltene fractions showed significant difference in absorbance at this wavelength with *irreversibly-adsorbed* fraction exhibiting the highest intensity [refer figure 3(b)] followed by *adsorbed* fraction. The

irreversibly-adsorbed fraction can hence be considered to contain the highest concentration of carbonyl, carboxylic acid or derivative groups.

The FTIR spectra for both *irreversibly-adsorbed*^{HCl} and *irreversibly-adsorbed*^{AA} is similar thereby indicating that the choice of acid used (HCl or acetic acid) in the final separation step does not affect the asphaltene structure. The slightly higher absorbance at 1700 cm^{-1} for *irreversibly-adsorbed*^{AA} fraction than the *irreversibly-adsorbed*^{HCl} fraction may be due to trace amounts of acetic acid remaining in the asphaltenes. It must however be noted that the main aim of performing fractionation using acetic acid was to study the possibility of reaction between asphaltenes and HCl under the fractionation conditions. The FTIR spectra of the *irreversibly adsorbed* fractions indicate that the use of HCl does not modify the chemical structure of asphaltenes compared with acetic acid.

To understand the effect of trace amount of $CaCO_3$ being present in the asphaltene samples, FTIR spectra were obtained for $CaCO_3$ as well as for a 90:10 (w/w) mixture of *whole* asphaltenes and $CaCO_3$. The corresponding spectra obtained between 2000 cm^{-1} and 600 cm^{-1} is shown in figure 4. It must be noted that only baseline correction was done for pure $CaCO_3$ spectra while normalization of spectra wasn't done. It can be clearly seen (figure 4) that a small amount of $CaCO_3$ in asphaltene sample does not influence the band at 1700 cm^{-1}. Similarly, the FTIR spectra of *control* asphaltenes (figure S1 in supplementary material) indicated a slight increase in absorbance at 1700 cm^{-1}. A slightly higher absorbance was observed in the intensity of peak for *control* asphaltenes than the *whole* asphaltenes. Moreover, the intensity of peak in *control* asphaltenes lies between the values of *bulk* and *adsorbed* asphaltenes. Even though this partially explains the reason for asphaltene fractions (*bulk, adsorbed* and *irreversibly-adsorbed*) having higher absorption intensity, it does not

however explain the significantly higher absorbance seen for *irreversibly-adsorbed* asphaltenes. This supports our earlier observation of higher presence of carbonyl, carboxylic acid or derivative groups in the *irreversibly-adsorbed* asphaltene fraction. The acidity of the asphaltene fractions could not be measured by total acid number (TAN) since high amounts of asphaltenes were needed and there was a problem of asphaltene precipitation in the TAN solvent mixture (toluene + isopropanol).

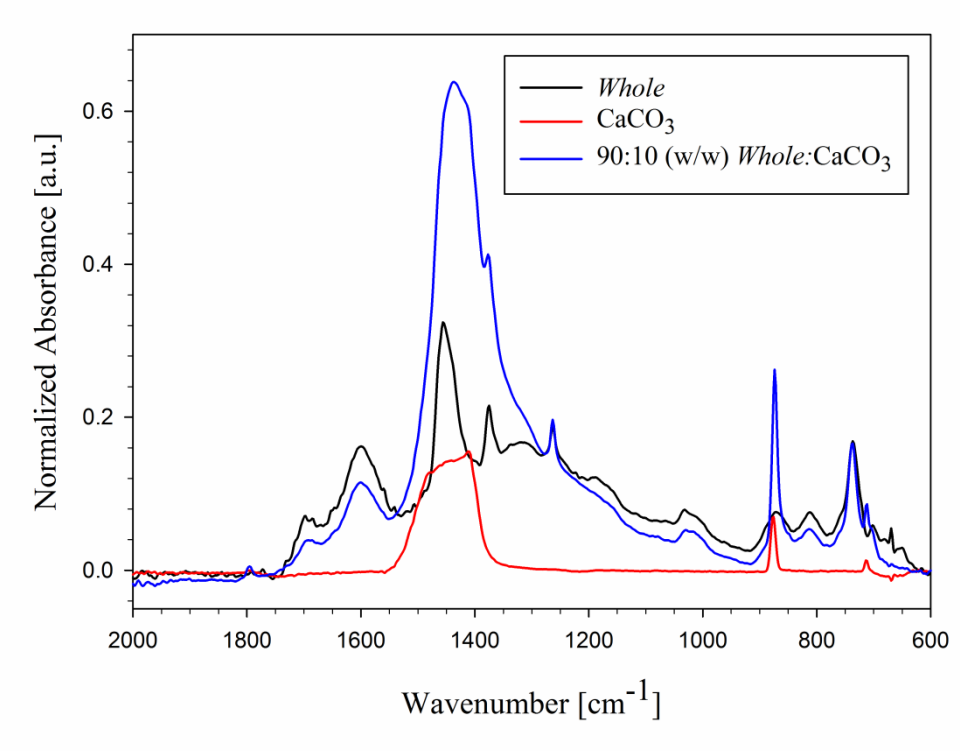

Figure 4: Normalized FTIR spectra for *whole* asphaltene, $CaCO_3$ and 90:10 (w/w) *whole* asphaltene: $CaCO_3$ mixture in the spectral range 2000 cm^{-1} and 600 cm^{-1}.

Figure 3(b) shows that there is a slight variation in intensity of the C=C aromatic stretching vibration at 1600 cm^{-1} and $–CH_3$ bending vibration at 1380 cm^{-1}. among the asphaltene fractions. A significant difference in absorption at 1460 cm^{-1} (corresponds to $–CH_2–$ bending vibration) was however observed with *bulk* asphaltene fraction showing the highest intensity. However, carbonate group also shows a broad and intense absorption band in the spectral

range 1490 cm^{-1} - 1410 cm^{-1} and a weak absorption band at 880 cm^{-1} - 860 cm^{-1} range.[55] This can also be clearly observed in figure 4 where the presence of $CaCO_3$ in whole asphaltene leads to a higher absorption at the spectral ranges mentioned. Thus the higher peak intensity observed at 1460 cm^{-1} for *bulk* fraction could be attributed to $CaCO_3$ contamination. The band around 1030 cm^{-1} is generally due to presence of sulfoxide group.[56] Presence of sulfoxide groups in asphaltenes could be due to oxidation.[57] All the asphaltene fractions showed absorbance at this wavenumber with *adsorbed* fraction showing the highest intensity. Absorption bands observed between 900 cm^{-1} and 700 cm^{-1} are due to different aromatic C-H bending deformations.[58] The band around 880 cm^{-1} indicates the presence of highly substituted aromatic structure[59] and this was found to be highest for *bulk* fraction and lowest for fraction *irreversibly-adsorbed*^{HCl}. Again, the higher absorbance intensity for *bulk* fraction at this wavenumber could be due to the $CaCO_3$ contamination.

3.4 Asphaltene adsorption by QCM

Figure 5 represents typical results obtained by QCM based on the procedure described in section 2.7. The instrument gives the frequency change and dissipation for overtones n=1, 3, 5, 7, 9, 11 and 13. The frequency change values corresponding to natural frequency (n=1) are generally not considered since it is sensitive to changes in the flow of bulk solution.[60] In figure 5, it can be observed that the dissipation change corresponding to 3rd overtone (n=3) is also sensitive to flow changes. The decrease in frequency when asphaltene solutions are injected is an indication of adsorption of asphaltenes onto the stainless steel surface. The data shows that we reach a plateau (i.e., a frequency change of less than 0.2 Hz during waiting time of 5 minutes) before every incremental of solution injected. Injection of xylene after injection of 1.5 g/L asphaltene solution was done to wash away the loosely bound asphaltenes. The frequency increases and dissipation change decreases during the xylene

washing. It can be seen that the overtones in frequency show negligible spreading and the dissipation changes are very small (close of zero). This indicates that a rigid layer has been formed.[61] Hence Sauerbrey's relation (equation 1) is valid and can be used to calculate the mass adsorbed onto surface.

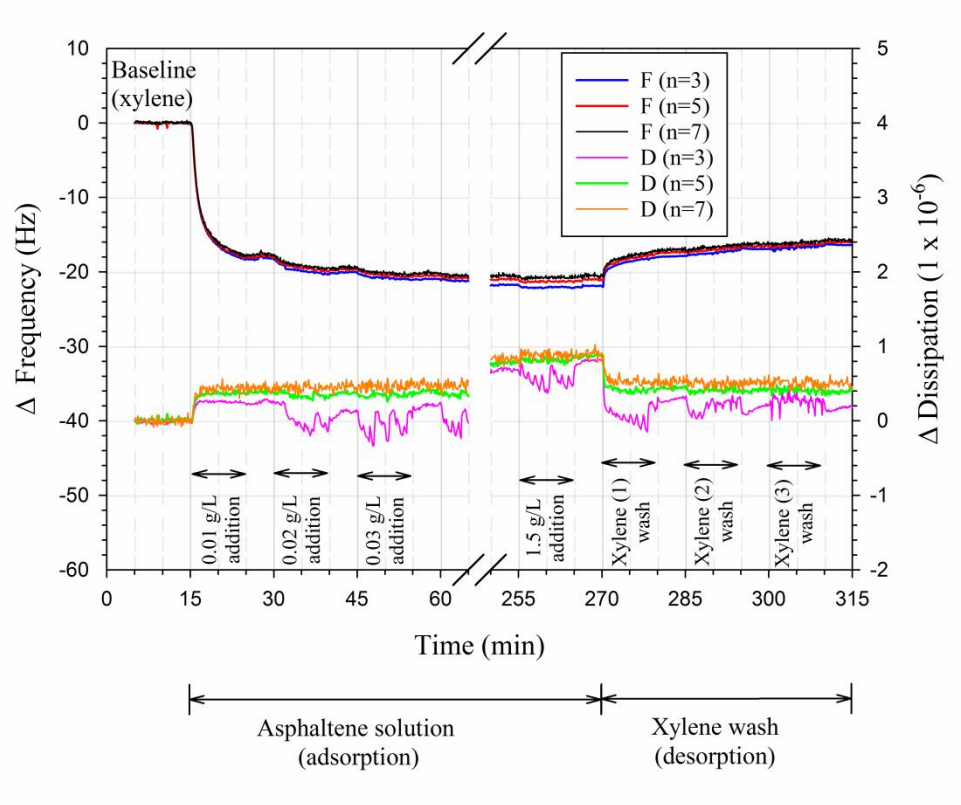

Figure 5: Frequency and dissipation changes for adsorption of *whole* asphaltenes solution in xylene onto stainless steel. Solutions were injected for 10 min at a flowrate of 50uL/min. The waiting time between injections was 5 min. F represents the frequency, D the dissipation and n the overtone number.

A comparison of the asphaltene mass adsorbed onto stainless steel at different overtone numbers (n = 3, 5, 7) is given in table 7. The mass adsorbed at different overtones are very similar thereby indicating the formation of rigid layer[62]. It should be noted that different overtones have different surface sensitivities. The higher overtones are more sensitive to changes in the film properties close to the surface since the decay length of acoustic waves

used in overtones decreases with increasing overtone number.[62] In the subsequent discussions, the frequency and dissipation change values corresponding to 5th overtone are reported.

Asphaltene adsorbed mass	Overtone number (n)		
	3	5	7
Plateau value before xylene wash (mg/m^2)	3.4	3.4	3.3
Plateau value after xylene wash (mg/m^2)	2.9	2.8	2.8

Table 7: Amount of *whole* asphaltenes adsorbed at different overtones numbers (n = 3, 5, 7).

Figure 6(a) shows the frequency and dissipation changes due to adsorption of the *whole* asphaltenes on stainless steel surface.

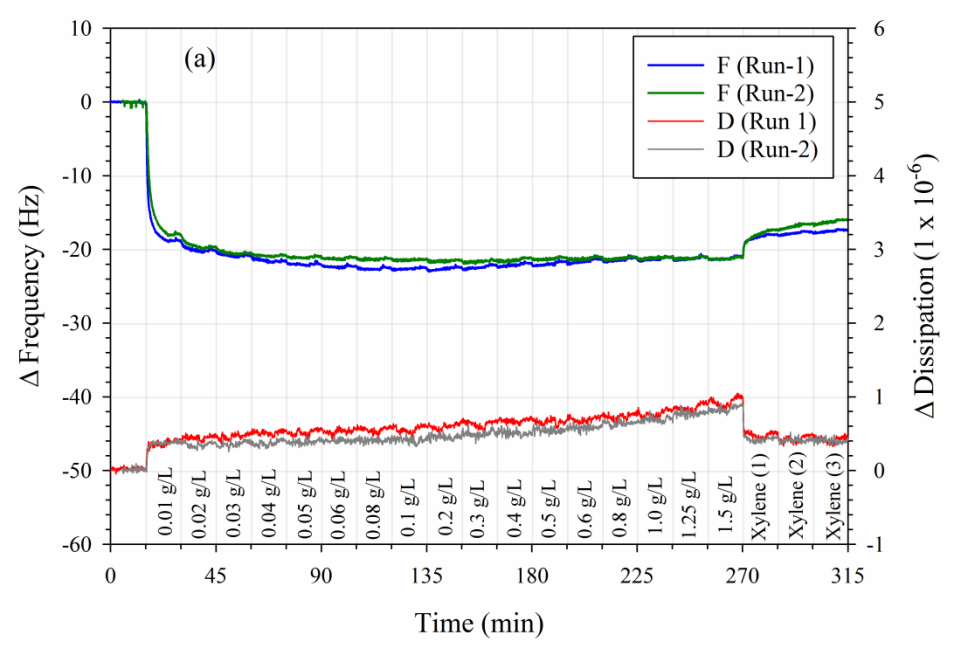

Figure 6(a): Adsorption of *whole* asphaltenes onto stainless steel for 5th overtone for two independent experiments. Asphaltene solutions in xylene from concentrations 0.01 g/L to 1.5 g/L were injected stepwise.

Initially, changes in frequency are observed when solutions of higher concentrations are injected. This is due to increased asphaltene adsorption with higher solution concentrations. Then, the frequency change becomes negligible for injections of asphaltene solutions higher than 0.05 g/L concentration thereby indicating that the surface is saturated with asphaltenes. The dissipation changes observed are very small (lower than 10^{-6}) thereby indicating the formation of a rigid layer.

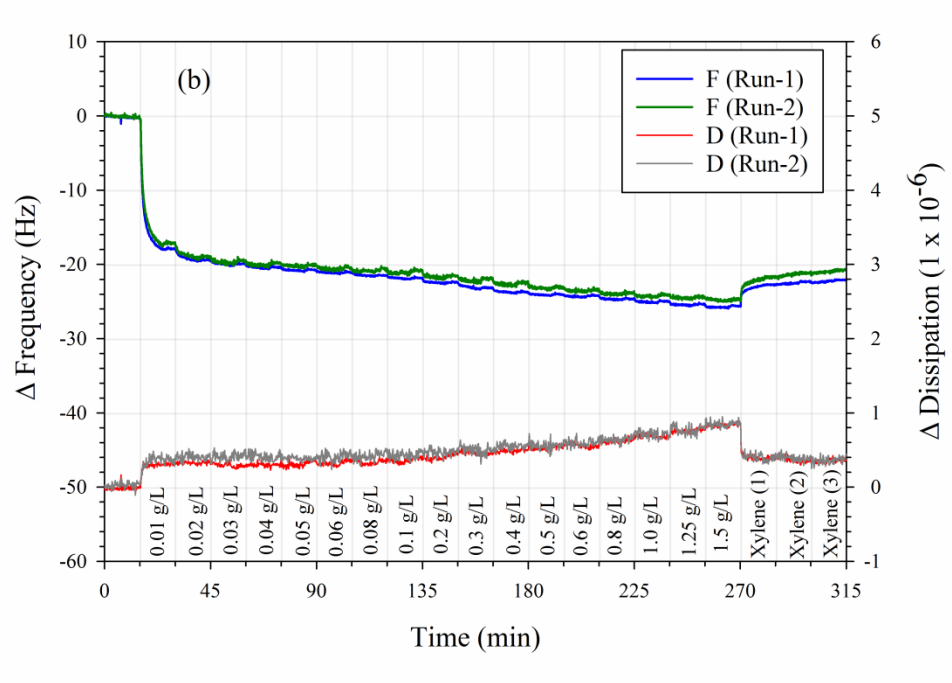

Figure 6(b): Adsorption of *bulk* asphaltenes fraction onto stainless steel for 5th overtone for two independent experiments.

The adsorption of *bulk* asphaltenes fraction on stainless steel is shown in figure 6(b). It can be noticed that the frequency change does not reach a constant value for the most concentrated solution tested of *bulk* asphaltenes fraction. This indicates that saturation of surface was not achieved within the concentration range tested. The dissipation change is again very small (10^{-6} at most) and hence the asphaltene layer formed by *bulk* fraction can be considered to be rigid. Both the asphaltene solutions (*whole* and *bulk*) exhibited good experimental reproducibility. Figure 6(c) represents the adsorption of *adsorbed* asphaltenes fraction. The

adsorbed fraction also does not show a saturation concentration within the tested concentration range on the stainless steel surface. The experiments show reasonable reproducibility at higher concentrations. The dissipation change observed is lower than 1.4 x 10^{-6}, thereby indicating that *adsorbed asphaltenes* fraction forms a rigid layer on the surface.

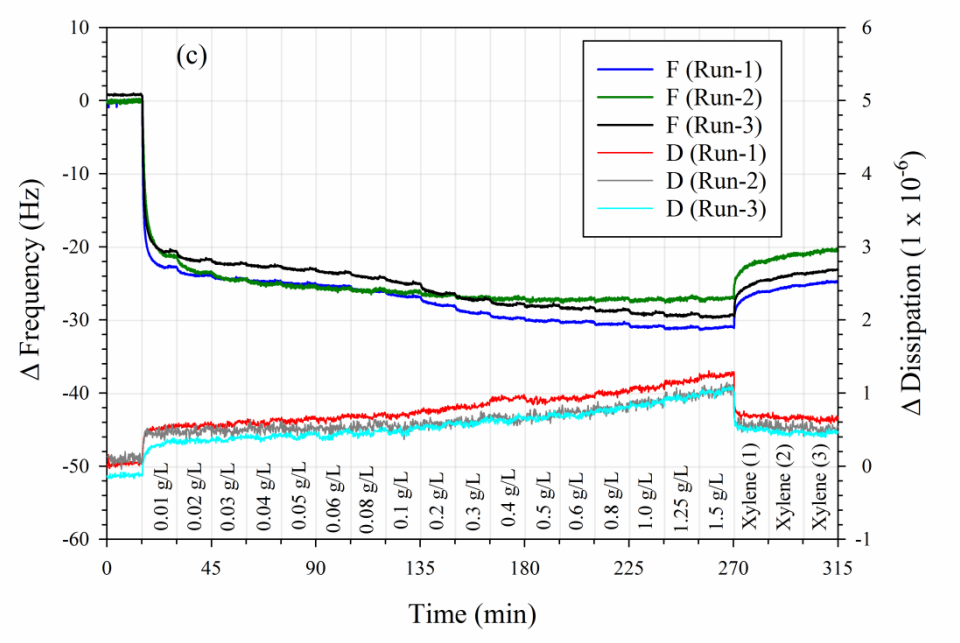

Figure 6(c): Adsorption of *adsorbed* asphaltenes fraction onto stainless steel for 5th overtone for 3 independent experiments.

Figure 6(d) shows the plot obtained when solutions of *irreversibly-adsorbed*^{HCl} asphaltenes sub-fraction was injected into QCM. At low concentrations, the repeatability of experiments is reasonable, but at concentrations higher than 0.2 g/L, the experiments show weak reproducibility with respect to frequency vs time curve. This concentration also corresponds to steeper increase in the dissipation values. Indeed significant dissipation changes were also observed when asphaltene solutions of higher concentration are injected. Similar characteristics can be seen in figure 6(e) for the *irreversibly-adsorbed*^{AA} fraction (fraction obtained using acetic acid during separation instead of HCl). Even though the reproducibility is less at higher concentrations for *irreversibly-adsorbed* asphaltenes fraction, it can be

observed that this fraction shows much higher adsorption capability on stainless steel surface than compared to other fractions. Currently, we do not have an explanation for the less reproducibility observed with the irreversibly-adsorbed asphaltenes sub-fraction. The spreading of overtones for frequency was observed for *irreversibly-adsorbed*^{HCl} and *irreversibly-adsorbed*^{AA} asphaltenes fractions. The spreading of frequency overtones is an indication that the film formed is not rigid.[61]

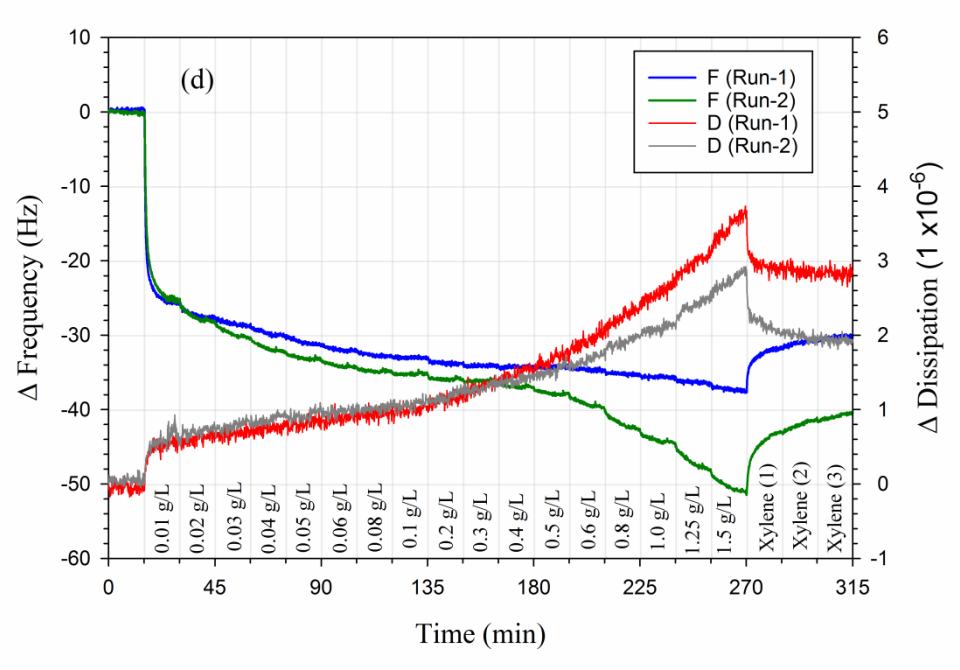

Figure 6 (d): Adsorption of *irreversibly-adsorbed*^{HCl} asphaltenes fraction onto stainless steel for 5th overtone for 2 independent experiments.

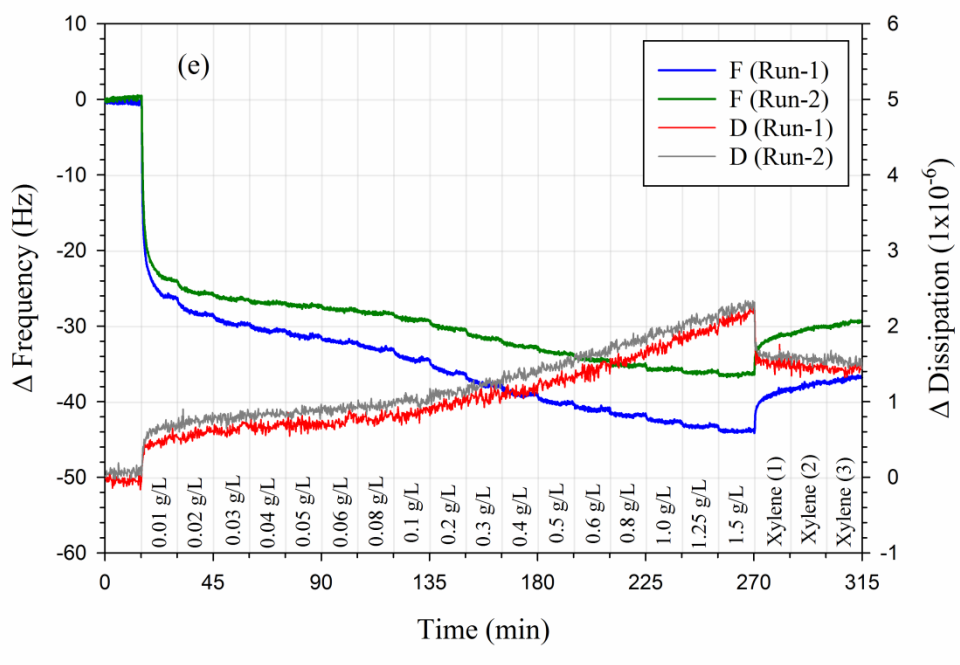

Figure 6 (e): Adsorption of *irreversibly-adsorbed*^{AA} asphaltenes fraction onto stainless steel for 5th overtone for 2 independent experiments.

The amount of asphaltenes adsorbed calculated from the Sauerbrey equation for the different asphaltene fractions (before xylene wash) is shown in figure 7. The *whole* asphaltenes showed the least adsorption (3.7 ± 0.1 mg/m^2) onto the stainless steel surface. The value obtained is slightly higher than the asphaltene saturation adsorption (2.7 mg/m^2) on stainless steel observed by Alboudwarej et al.[39] but lower than the asphaltene saturation adsorption (4.9 mg/m^2) on iron observed by Balabin et al.[46] The *bulk* asphaltenes fraction shows a slightly higher adsorption (4.4 ± 0.1 mg/m^2) followed by *adsorbed* asphaltenes fraction (5.2 ± 0.3 mg/m^2). The highest adsorption ability is shown by *irreversibly-adsorbed* fraction with HCl separated fraction (*irreversibly-adsorbed*^{HCl}) having Γ = 7.8 ± 1.1 mg/m^2 and acetic acid separated fraction (*irreversibly-adsorbed*^{AA}) having Γ = 7.1 ± 0.6 mg/m^2. This higher adsorbed amount and the fact that the slope of the variation of the dissipation with the concentration increases at asphaltene concentration of approximately 0.2 g/L point towards the formation of an adsorption multilayer at the interface. It should however be kept in mind

that the *irreversibly-adsorbed asphaltenes* fraction forms a non-rigid film and hence the adsorbed amount for this fraction calculated using Sauerbrey equation is not accurate. Iruthayaraj et al.[63] observed that the use of Sauerbrey relation to calculate adsorbed mass in non-rigid layers leads to under-prediction by a factor of 1.15 – 1.45 than compared to predictions by Voigt model[64].

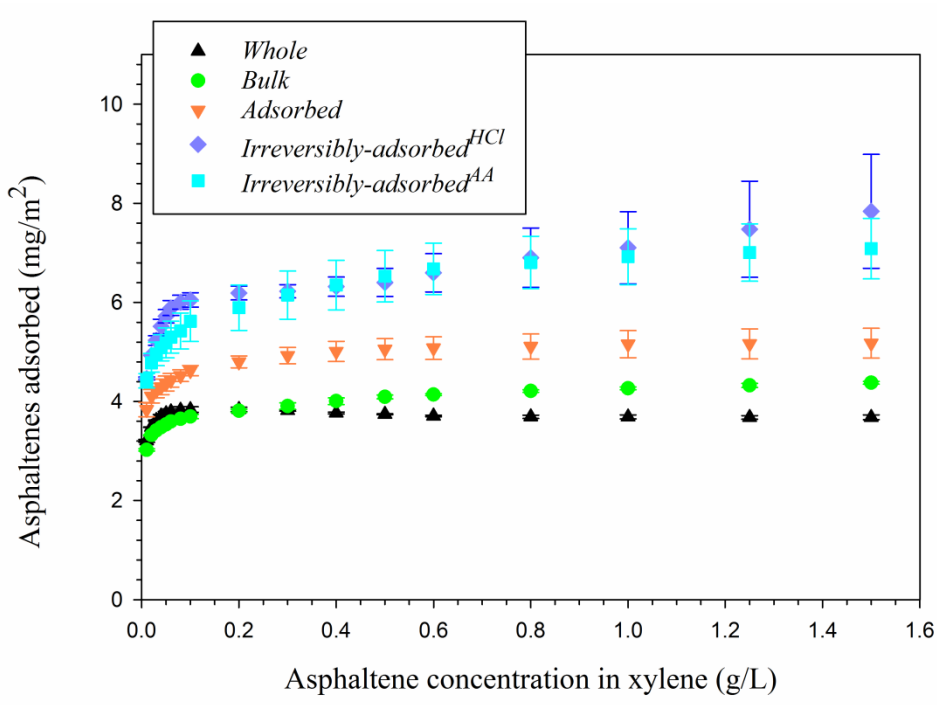

Figure 7: Amount of asphaltene fractions adsorbed on stainless steel based on 5th overtone.

The primary difference between the different asphaltene sub-fractions is the concentration of carbonyl, carboxylic acid or derivative groups (from FTIR analysis). The concentration of these groups in the sub-fractions follows the order *irreversibly-adsorbed* > *adsorbed* > *bulk* with *irreversibly-adsorbed* fraction showing a significantly higher presence of carbonyl, carboxylic acid or derivative groups compared to *adsorbed* and *bulk* fractions. This could be the reason for the asphaltene adsorbed amount following the same order (*irreversibly-adsorbed* > *adsorbed* > *bulk*). This reasoning is supported by the presence of carboxylic acids observed in adsorbed asphaltene layer on stainless steel based on XPS analysis by Abdallah

and Taylor[65]. It is also known that the interaction between asphaltenes and metal surface is limited by the number of available adsorption sites on the metal surface.[66] The XPS analysis from the manufacturer of stainless steel surface (table 3) used for QCM experiments indicates the presence of oxides of iron and chromium on the surface. Chromium is present in stainless steel in the form of chromium oxide (Cr_2O_3) and this passive layer prevents further oxidation of metal substrate.[67] Carboxylic acids however have an ability to interact with chromium (III) oxide and get adsorbed onto the surface.[68, 69] The highest adsorption observed with *irreversibly-adsorbed* asphaltene sub-fraction may be due to the high concentration of carboxylic acid groups present in them, thereby resulting in more interaction with the stainless steel surface. Another explanation can be put forward. As the adsorption of all the sub-fractions (*bulk, adsorbed* and *irreversibly-adsorbed*) are higher than the adsorption of *whole* asphaltenes, it can be deduced that it is unlikely that the concentration of some functional group obtained by fractionation would be the only factor to explain the order of adsorption (*irreversibly-adsorbed* > *adsorbed* > *bulk* > *whole*). It is likely that fractionation also modifies interactions between components in the asphaltene fractions thereby leading to stabilization of asphaltenes in the unfractionated asphaltene sample and hence would limit the adsorption onto stainless steel. Hence there is a need for further investigation of self-association properties of sub-fractions and to determine the raw formula using advanced techniques like FT-ICR-MS.

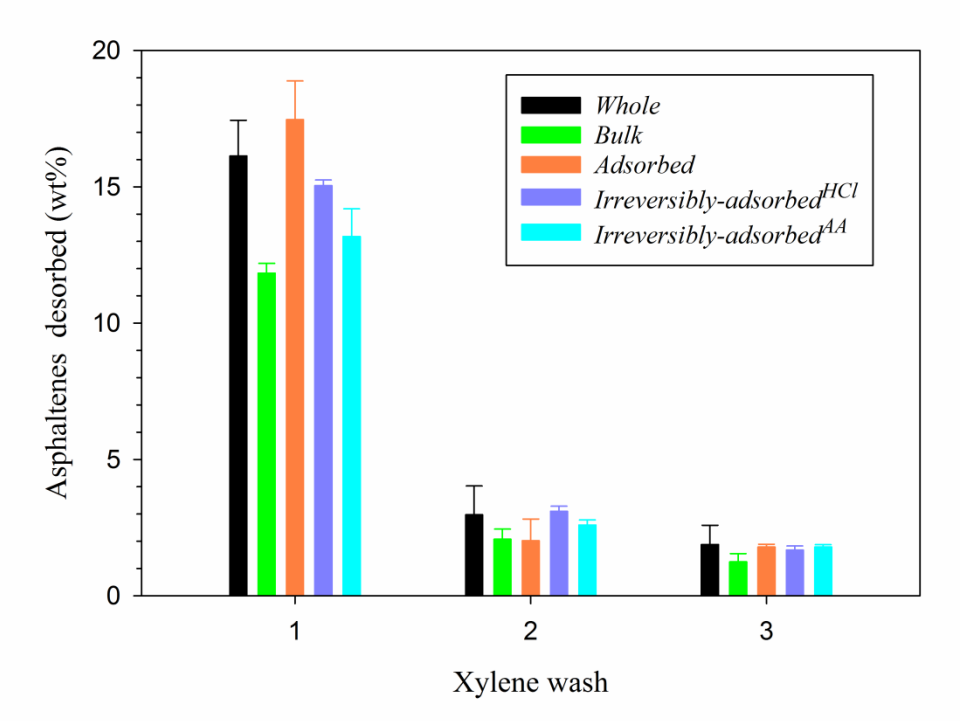

Figure 8: Asphaltene desorption from stainless steel surface during xylene washing.

The efficiency of xylene wash for desorption of asphaltenes (at the end of experiment) is shown in figure 8. Xylene was found to be ineffective in removing the asphaltenes completely from the surface. Most of the asphaltene desorption happens during the first xylene wash. The overall desorption was found to be in the range 15–25% (by weight) asphaltenes were desorbed during the xylene wash with the *bulk* sub-fraction showing the least desorption around 15% (by weight). This indicates that the asphaltene adsorption is quite strong onto the surface, but the narrow desorption range (15-25% by weight) indicates that the asphaltenes fractions show similar adsorption strength onto the stainless steel surface. Also, the choice of acid used (strong acid HCl or a weak acid acetic acid) for separation showed only a negligible effect on the structure and properties of the *irreversibly-adsorbed* asphaltene fraction.

4. CONCLUSIONS

A new procedure was developed to fractionate North Sea asphaltenes based on adsorption onto calcium carbonate and the properties of the sub-fractions were studied using elemental analysis, FTIR and QCM measurements. FTIR analysis indicated that the fractionation resulted in separating asphaltenes into fractions with differences in presence of carbonyl, carboxylic acid or derivative groups. The ability of the different fractions to adsorb onto stainless steel was measured using QCM. The *whole* asphaltenes exhibited the least adsorption (3.4 mg/m^2) onto stainless steel while the maximum adsorption (around 8 mg/m^2) was observed for *irreversibly-adsorbed* asphaltene sub-fraction containing the highest concentration of carbonyl, carboxylic acid or derivative groups. *Irreversibly-adsorbed* sub-fraction also showed the ability to form visco-elastic layers onto the metal surface and hence the adsorbed amount (calculated using Sauerbrey equation) is lower than actual values. This suggests the formation of multilayers of adsorbed asphaltenes. The asphaltene sub-fractions (*bulk*, *adsorbed* and *irreversibly-adsorbed*) did not show maximum saturation amount (Γ_{max}) within the concentration range tested (0.01 – 1.5 g/L). The fact that the unfractionated (or *whole*) asphaltenes showed the least adsorption capability suggested that the asphaltene sub-fractions tend to interact among themselves thereby reducing the adsorption. Desorption of asphaltenes using xylene was found to be ineffective with only 15-25% (by weight) asphaltenes removed, thereby indicating a strong interaction between asphaltenes and stainless steel surface. More investigation i.e., self-association properties and mass resolution by techniques like FT-ICR-MS needs to be done to obtain in-depth understanding about the mechanism governing the asphaltene adsorption onto metal surfaces.

5. AUTHOR INFORMATION

Corresponding author

*Email address: sreedhar.subramanian@ntnu.no

Tel: (+47) 73 59 41 59

6. ACKNOWLEDGEMENT

The authors thank JIP Asphaltene consortium “Improved Mechanism of Asphaltene Deposition, Precipitation and Fouling to Minimize Irregularities in Production and Transport – A Cost Effective and Environmentally Friendly Approach (NFR PETROMAKS, Grant number - 234112)”, consisting of Ugelstad Laboratory (NTNU, Norway), University of Alberta (Canada), University of Pau (France), Federal University of Paraná (Brazil) and funded by Norwegian Research Council and the following industrial sponsors – AkzoNobel, British Petroleum, Canada Natural Resources, Nalco Champion, Petrobras, Statoil and Total.

7. REFERENCES

[1] J. Sjoblom, S. Simon, Z. Xu, Model molecules mimicking asphaltenes, Advances in colloid and interface science, 218 (2015) 1-16.

[2] O.C. Mullins, The Asphaltenes, Annual Review of Analytical Chemistry, 4 (2011) 393-418.

[3] J.G. Speight, The chemical and physical structure of petroleum: effects on recovery operations, Journal of Petroleum Science and Engineering, 22 (1999) 3-15.

[4] H. Groenzin, O.C. Mullins, Asphaltene Molecular Size and Structure, The Journal of Physical Chemistry A, 103 (1999) 11237-11245.

[5] O.C. Mullins, H. Sabbah, J. Eyssautier, A.E. Pomerantz, L. Barré, A.B. Andrews, Y. Ruiz-Morales, F. Mostowfi, R. McFarlane, L. Goual, R. Lepkowicz, T. Cooper, J. Orbulescu, R.M. Leblanc, J. Edwards, R.N. Zare, Advances in Asphaltene Science and the Yen–Mullins Model, Energy & Fuels, 26 (2012) 3986-4003.

[6] J.D. McLean, P.K. Kilpatrick, Comparison of Precipitation and Extrography in the Fractionation of Crude Oil Residua, Energy & Fuels, 11 (1997) 570-585.

[7] H.W. Yarranton, J.H. Masliyah, Molar mass distribution and solubility modeling of asphaltenes, AIChE Journal, 42 (1996) 3533-3543.

[8] V. Nalwaya, V. Tantayakom, P. Piumsomboon, S. Fogler, Studies on Asphaltenes through Analysis of Polar Fractions, Industrial & Engineering Chemistry Research, 38 (1999) 964-972.

[9] T.J. Kaminski, H.S. Fogler, N. Wolf, P. Wattana, A. Mairal, Classification of Asphaltenes via Fractionation and the Effect of Heteroatom Content on Dissolution Kinetics, Energy & Fuels, 14 (2000) 25-30.

[10] H. Groenzin, O.C. Mullins, S. Eser, J. Mathews, M.-G. Yang, D. Jones, Molecular Size of Asphaltene Solubility Fractions, Energy & Fuels, 17 (2003) 498-503.

[11] E. Buenrostro-Gonzalez, S.I. Andersen, J.A. Garcia-Martinez, C. Lira-Galeana, Solubility/Molecular Structure Relationships of Asphaltenes in Polar and Nonpolar Media, Energy & Fuels, 16 (2002) 732-741.

[12] A.M. Kharrat, New Approach for Characterizing Heavy Oils, Energy & Fuels, 22 (2008) 1402-1403.

[13] A.M. Kharrat, Characterization of Canadian Heavy Oils Using Sequential Extraction Approach, Energy & Fuels, 23 (2009) 828-834.

[14] J. Marques, I. Merdrignac, A. Baudot, L. Barré, D. Guillaume, D. Espinat, S. Brunet, Séparation des asphaltènes par nano et ultrafiltration – Comparaison avec la méthode de floculation, Oil & Gas Science and Technology - Rev. IFP, 63 (2008) 139-149.

[15] M. Fossen, H. Kallevik, K.D. Knudsen, J. Sjöblom, Asphaltenes Precipitated by a Two-Step Precipitation Procedure. 1. Interfacial Tension and Solvent Properties, Energy & Fuels, 21 (2007) 1030-1037.

[16] M. Fossen, H. Kallevik, K.D. Knudsen, J. Sjöblom, Asphaltenes Precipitated by a Two-Step Precipitation Procedure. 2. Physical and Chemical Characteristics, Energy & Fuels, 25 (2011) 3552-3567.

[17] X. Yang, H. Hamza, J. Czarnecki, Investigation of Subfractions of Athabasca Asphaltenes and Their Role in Emulsion Stability, Energy & Fuels, 18 (2004) 770-777.

[18] S. Lawrence, L.Y. Zhang, Z. Xu, J. Masliyah, Langmuir and Langmuir-Blodgett Asphaltene Films at Heptane-water Interface, The Canadian Journal of Chemical Engineering, 82 (2004) 821-828.

[19] D. Fenistein, L. Barré, Experimental measurement of the mass distribution of petroleum asphaltene aggregates using ultracentrifugation and small-angle X-ray scattering, Fuel, 80 (2001) 283-287.

[20] L. Barré, S. Simon, T. Palermo, Solution Properties of Asphaltenes, Langmuir, 24 (2008) 3709-3717.

[21] H.B. Jemison, R.R. Davison, C.J. Glover, J.A. Bullin, Fractionation of Asphalt Materials by using Supercritical Cyclohexane and Pentane, Fuel Science and Technology International, 13 (1995) 605-638.

[22] T.M. Ignasiak, L. Kotlyar, N. Samman, D.S. Montgomery, O.P. Strausz, Preparative gel permeation chromatography of Athabasca asphaltene and the relative polymer-forming propensity of the fractions, Fuel, 62 (1983) 363-369.

[23] K.M. Semple, N. Cyr, P.M. Fedorak, D.W.S. Westlake, Characterization of asphaltenes from Cold Lake heavy oil: variations in chemical structure and composition with molecular size, Canadian Journal of Chemistry, 68 (1990) 1092-1099.

[24] K.D. Bartle, M.J. Mulligan, N. Taylor, T.G. Martin, C.E. Snape, Molecular mass calibration in size-exclusion chromatography of coal derivatives, Fuel, 63 (1984) 1556-1560.

[25] C.Z. Li, K.D. Bartle, R. Kandiyoti, Characterization of tars from variable heating rate pyrolysis of maceral concentrates, Fuel, 72 (1993) 3-11.

[26] A.A. Herod, S.-F. Zhang, B.R. Johnson, K.D. Bartle, R. Kandiyoti, Solubility Limitations in the Determination of Molecular Mass Distributions of Coal Liquefaction and Hydrocracking Products: 1-Methyl-2-pyrrolidinone as Mobile Phase in Size Exclusion Chromatography, Energy & Fuels, 10 (1996) 743-750.

[27] E. Al-Muhareb, T.J. Morgan, A.A. Herod, R. Kandiyoti, Characterization of Petroleum Asphaltenes by Size Exclusion Chromatography, UV-fluorescence and Mass Spectrometry, Petroleum Science and Technology, 25 (2007) 81-91.

[28] M. Millan, M. Behrouzi, F. Karaca, T.J. Morgan, A.A. Herod, R. Kandiyoti, Characterising high mass materials in heavy oil fractions by size exclusion chromatography and MALDI-mass spectrometry, Catalysis Today, 109 (2005) 154-161.

[29] S. Badre, C. Carla Goncalves, K. Norinaga, G. Gustavson, O.C. Mullins, Molecular size and weight of asphaltene and asphaltene solubility fractions from coals, crude oils and bitumen, Fuel, 85 (2006) 1-11.

[30] B.E. Ascanius, D.M. Garcia, S.I. Andersen, Analysis of Asphaltenes Subfractionated by N-Methyl-2-pyrrolidone, Energy & Fuels, 18 (2004) 1827-1831.

[31] C. Berrueco, S. Venditti, T.J. Morgan, P. Álvarez, M. Millan, A.A. Herod, R. Kandiyoti, Calibration of Size-Exclusion Chromatography Columns with 1-Methyl-2-pyrrolidinone (NMP)/Chloroform Mixtures as Eluent: Applications to Petroleum-Derived Samples, Energy & Fuels, 22 (2008) 3265-3274.

[32] G. Piro, L.B. Canonico, G. Galbariggi, L. Bertero, C. Carniani, Asphaltene Adsorption Onto Formation Rock: An Approach to Asphaltene Formation Damage Prevention, SPE Production & Facilities, 11 (1996) 156-160.

[33] J.S. Buckley, Wetting Alteration of Solid Surfaces by Crude Oils and Their Asphaltenes, Oil & Gas Science and Technology - Rev. IFP, 53 (1998) 303-312.

[34] A. Hammami, J. Ratulowski, Precipitation and Deposition of Asphaltenes in Production Systems: A Flow Assurance Overview, in: O. Mullins, E. Sheu, A. Hammami, A. Marshall (Eds.) Asphaltenes, Heavy Oils, and Petroleomics, Springer New York (2007), pp. 617-660.

[35] A.H. Kamran Akbarzadeh, Abdel Kharrat, Dan Zhang, Stephan Allenson, Jefferson Creek, Shah Kabir, A. Jamaluddin, Alan G. Marshall, Ryan Rodgers, Oliver C. Mullins, Trond Solbakken, Asphaltenes—Problematic but Rich in Potential, Oil Field Review, (2007) 22-43.

[36] P. Ekholm, E. Blomberg, P. Claesson, I.H. Auflem, J. Sjöblom, A. Kornfeldt, A Quartz Crystal Microbalance Study of the Adsorption of Asphaltenes and Resins onto a Hydrophilic Surface, Journal of Colloid and Interface Science, 247 (2002) 342-350.

[37] D. Dudášová, A. Silset, J. Sjöblom, Quartz Crystal Microbalance Monitoring of Asphaltene Adsorption/Deposition, Journal of Dispersion Science and Technology, 29 (2008) 139-146.

[38] K. Xie, K. Karan, Kinetics and Thermodynamics of Asphaltene Adsorption on Metal Surfaces: A Preliminary Study†, Energy & Fuels, 19 (2005) 1252-1260.

[39] H. Alboudwarej, D. Pole, W.Y. Svrcek, H.W. Yarranton, Adsorption of Asphaltenes on Metals, Industrial & Engineering Chemistry Research, 44 (2005) 5585-5592.

[40] D. Dudášová, S. Simon, P.V. Hemmingsen, J. Sjöblom, Study of asphaltenes adsorption onto different minerals and clays: Part 1. Experimental adsorption with UV depletion detection, Colloids and Surfaces A: Physicochemical and Engineering Aspects, 317 (2008) 1-9.

[41] S.T. Dubey, M.H. Waxman, Asphaltene Adsorption and Desorption From Mineral Surfaces, SPE Reservoir Engineering, 6 (1991) 389-395.

[42] S. Acevedo, J. Castillo, A. Fernández, S. Goncalves, M.A. Ranaudo, A Study of Multilayer Adsorption of Asphaltenes on Glass Surfaces by Photothermal Surface Deformation. Relation of This Adsorption to Aggregate Formation in Solution, Energy & Fuels, 12 (1998) 386-390.

[43] A.W. Marczewski, M. Szymula, Adsorption of asphaltenes from toluene on mineral surface, Colloids and Surfaces A: Physicochemical and Engineering Aspects, 208 (2002) 259-266.

[44] S. Acevedo, M.A. Ranaudo, G. Escobar, L. Gutiérrez, P. Ortega, Adsorption of asphaltenes and resins on organic and inorganic substrates and their correlation with precipitation problems in production well tubing, Fuel, 74 (1995) 595-598.

[45] S. Acevedo, M.A. Ranaudo, C. García, J. Castillo, A. Fernández, Adsorption of Asphaltenes at the Toluene−Silica Interface: A Kinetic Study, Energy & Fuels, 17 (2003) 257-261.

[46] R.M. Balabin, R.Z. Syunyaev, T. Schmid, J. Stadler, E.I. Lomakina, R. Zenobi, Asphaltene Adsorption onto an Iron Surface: Combined Near-Infrared (NIR), Raman, and AFM Study of the Kinetics, Thermodynamics, and Layer Structure, Energy & Fuels, 25 (2011) 189-196.

[47] M. Castro, J.L.M. de la Cruz, E. Buenrostro-Gonzalez, S. López-Ramírez, A. Gil-Villegas, Predicting adsorption isotherms of asphaltenes in porous materials, Fluid Phase Equilibria, 286 (2009) 113-119.

[48] S. M. L, K.I.M. S. S, S. F, S. O. P, Structure-Related Properties of Athabasca Asphaltenes and Resins as Indicated by Chromatographic Separation, Chemistry of Asphaltenes, American Chemical Society1982, pp. 83-118.

[49] M.A. Francisco, J.G. Speight, Asphaltene Characterization by a Nonspectroscopic Method, Abstracts of papers of the American Chemical Society, American Chemical Society, Washington, DC 20036, 1984, pp. 5-Fuel.

[50] J.G. Speight, Chapter 2 Chemical and Physical Studies of Petroleum Asphaltenes, in: T.F. Yen, G.V. Chilingarian (Eds.) Developments in Petroleum Science, Elsevier1994, pp. 7-65.

[51] A.L. Nenningsland, S. Simon, J. Sjöblom, Surface Properties of Basic Components Extracted from Petroleum Crude Oil, Energy & Fuels, 24 (2010) 6501-6505.

[52] W.R. Glomm, T. Vrålstad, G. Øye, J. Sjøblom, M.W. Støcker, A direct sol-gel synthesis method for incorporation of transition metals into the framework of ordered mesoporous materials, Journal of dispersion science and technology, 26 (2005) 95-104.

[53] G. Sauerbrey, Verwendung von Schwingquarzen zur Wägung dünner Schichten und zur Mikrowägung, Z. Physik, 155 (1959) 206-222.

[54] M. Rodahl, F. Höök, A. Krozer, P. Brzezinski, B. Kasemo, Quartz crystal microbalance setup for frequency and Q-factor measurements in gaseous and liquid environments, Review of Scientific Instruments, 66 (1995) 3924-3930.

[55] J. Coates, Interpretation of Infrared Spectra, A Practical Approach, in: M. R.A. (Ed.) Encyclopedia of Analytical Chemistry, John Wiley & Sons Ltd, Chichester, 2000, pp. 10815 - 10837.

[56] B. Gaweł, M. Eftekhardadkhah, G. Øye, Elemental Composition and Fourier Transform Infrared Spectroscopy Analysis of Crude Oils and Their Fractions, Energy & Fuels, 28 (2014) 997-1003.

[57] P.M. Spiecker, K.L. Gawrys, P.K. Kilpatrick, Aggregation and solubility behavior of asphaltenes and their subfractions, Journal of Colloid and Interface Science, 267 (2003) 178-193.

[58] L.V. Castro, F. Vazquez, Fractionation and Characterization of Mexican Crude Oils, Energy & Fuels, 23 (2009) 1603-1609.

[59] B. Sharma, C. Sharma, O. Tyagi, S. Bhagat, S. Erhan, Structural characterization of asphaltenes and ethyl acetate insoluble fractions of petroleum vacuum residues, Petroleum science and technology, 25 (2007) 121-139.

[60] A. Mechler, S. Praporski, K. Atmuri, M. Boland, F. Separovic, L.L. Martin, Specific and Selective Peptide-Membrane Interactions Revealed Using Quartz Crystal Microbalance, Biophysical Journal, 93 (2007) 3907-3916.

[61] M. Tavakkoli, S.R. Panuganti, F.M. Vargas, V. Taghikhani, M.R. Pishvaie, W.G. Chapman, Asphaltene Deposition in Different Depositing Environments: Part 1. Model Oil, Energy & Fuels, 28 (2014) 1617-1628.

[62] Á. Piñeiro, Wiley Series on Surface and Interfacial Chemistry : Proteins in Solution and at Interfaces : Methods and Applications in Biotechnology and Materials Science, John Wiley & Sons, Somerset, NJ, USA, 2013.

[63] J. Iruthayaraj, G. Olanya, P.M. Claesson, Viscoelastic Properties of Adsorbed Bottle-brush Polymer Layers Studied by Quartz Crystal Microbalance — Dissipation Measurements, The Journal of Physical Chemistry C, 112 (2008) 15028-15036.

[64] M. Rodahl, B. Kasemo, On the measurement of thin liquid overlayers with the quartz-crystal microbalance, Sensors and Actuators, A: Physical, 54 (1996) 448-456.

[65] W.A. Abdallah, S.D. Taylor, Surface characterization of adsorbed asphaltene on a stainless steel surface, Nuclear Instruments and Methods in Physics Research Section B: Beam Interactions with Materials and Atoms, 258 (2007) 213-217.

[66] N. Hosseinpour, A.A. Khodadadi, A. Bahramian, Y. Mortazavi, Asphaltene Adsorption onto Acidic/Basic Metal Oxide Nanoparticles toward in Situ Upgrading of Reservoir Oils by Nanotechnology, Langmuir, 29 (2013) 14135-14146.

[67] K.A. Habib, M.S. Damra, J.J. Saura, I. Cervera, J. Bellés, Breakdown and Evolution of the Protective Oxide Scales of AISI 304 and AISI 316 Stainless Steels under High-Temperature Oxidation, International Journal of Corrosion, 2011 (2011) 10.

[68] R.A. Sheldon, H. van Bekkum, Catalytic Hydrogenation and Dehydrogenation, Fine Chemicals through Heterogeneous Catalysis, Wiley-VCH Verlag GmbH2007, pp. 351-471.

[69] E. Johansson, L. Nyborg, XPS study of carboxylic acid layers on oxidized metals with reference to particulate materials, Surface and Interface Analysis, 35 (2003) 375-381.